European Polymer Journal 46 (2010) 1660–1670

Contents lists available at ScienceDirect

European Polymer Journal

journal homepage: www.elsevier.com/locate/europolj

Macromolecular Nanotechnolgy

Micro-contact printing of poly(3-hexylthiophene) on silicon oxide: Effect of stamp stretching

Guido Scavia [a,*], William Porzio [a], Silvia Destri [a], Luisa Barba [b], Gianmichele Arrighetti [b]

[a] ISMAC, CNR, Via E. Bassini 15, 20133 Milano, Italy
[b] Istituto di Cristallografia-Sincrotrone Elettra, Strada Statale 14-Km 163, 5 Area Science Park, 34012 Basovizza, Trieste, Italy

ARTICLE INFO

Article history:
Received 23 February 2010
Received in revised form 17 May 2010
Accepted 31 May 2010
Available online 2 June 2010

Keywords:
Poly(3-hexylthiophene) film
Micro-contact printing
Structure and morphology
Atomic force microscopy

ABSTRACT

Micro-contact printing (μCP) has been applied to deposit poly(3-hexylthiophene) (P3HT) layer onto silicon oxide substrate from a polydimethylsiloxane (PDMS) stamp. The effect of the stamp stretching onto the corresponding printed P3HT layer has been analysed both from morphological (AFM) and from structural (XRD) points of view. Results show an orienting effect of the stretching towards the P3HT ultimate morphological units (i.e. fibrils) along the stretching direction. The influence of other variables involved in the deposition (substrate polarity/apolarity, mechanical pressure onto the stamp) have been studied and reported.

1. Introduction

In the development of an organic electronic device, the patterning of an appropriate substrate with lithographic techniques represents one of the key steps both for making contacts and for positioning the active layers only in particular areas of the same substrate. In this concern, soft lithography such as micro-contact printing (μCP) has some significant advantages as compared to the more conventional lithography, namely its versatility, low cost and ability to transfer a particular self-assembled monolayer (SAM) pattern with nanometer resolution to a substrate [1–12]. In μCP the layer to be deposited is directly released from an elastomeric stamp, e.g. polydimethylsiloxane (PDMS), to the substrate in solvent-free conditions, taking advantage of the interaction (physi- or chemi-sorption) between the layer and the final substrate to the detriment of the interaction forces initially keeping it adsorbed to the stamp [13–15]. PDMS not only acts as the carrier of the layer but also can transfer to it a predetermined pattern previously 'written' onto the stamp itself. One of the principal uses of μCP is the production of SAM layers of alkyl thioles onto gold [16–18], silanizers such as octadecyltrichlorosilane (OTS) on silicon oxide [19,20], phosphonic acid [21], polymer [22,23], and metals on silicon oxide [24,25]. Nanowires of different materials have been deposited by using contact printing [26]. For all these printed materials, the predefined pattern generally consists of rows with periods up to few nanometers for bio- or optoelectronic applications [18,27,28]. The printed layer not necessarily needs to chemisorb onto the substrate but a physisorption is sufficient if the interaction with the substrate results stronger as compared with that occurring with the PDMS mold [29,30]. μCP has also been used to print metallic patterns with a modified electrical technique (e-μCP) [31,32] and to print Au metal particles [12,33]. For organic materials, μCP depositions of a homogeneous layer of polymers for OFET applications such as poly-3-hexylthiophene (P3HT) [34–37] has been carried out as an alternative to the spin coating method commonly used for this material [38–48]. In the case of a P3HT deposition with μCP, two printing methods have been followed: (1) Indirect method: (a) deposition by spin coating of the P3HT layer onto a first substrate (OTS functionalized silicon oxide), (b) use PDMS to peel off the P3HT layer from

* Corresponding author. Tel.: +39 02 23699745; fax: +39 02 70636400.
E-mail address: guido.scavia@ismac.cnr.it (G. Scavia).

0014-3057/$ - see front matter © 2010 Elsevier Ltd. All rights reserved.
doi:10.1016/j.eurpolymj.2010.05.010

the first substrate, (c) transfer the film to the final substrate by simply pressing it for few seconds [36,37]. (2) Direct method: place a drop of the P3HT solution onto stamp and then press the stamp onto the final substrate as in 1c) [35].

The main goal of this article is a new use of μCP method not only to print a P3HT layer in a reproducible way but also to exploit the elastic properties of the PDMS to stretch the adsorbed P3HT layer and to demonstrate at a nanometric level that the corresponding effect onto P3HT is to produce an orientation of the singular P3HT fibrils along the stretching direction. This could have important electronic and device implications since P3HT fibril orientation, in its turn, has been demonstrated [49,50] to give rise to an improvement to the overall mobility.

In particular, this work is organized in the following steps:

- Morphological and structural effects determined by the stretching and/or the mechanical pressure of the PDMS stamp onto the P3HT compared to the non-stretched case.
- Possible role of the substrate polar/apolar character on the P3HT morphology.

The techniques used to pursue the above goals are atomic force microscopy (AFM) and synchrotron X-ray diffraction (XRD).

2. Experimental

2.1. Micro-contact printing procedure

The μCP procedure consists in a P3HT peeling off with PDMS from P3HT/OTS and printing onto the substrate such as SiO_x and OTS/SiO_x. Fig. 1 shows the steps of the printing procedure. In phase1 P3HT (5 mg/cc toluene solution) is deposited by spin coating onto OTS functionalized silicon oxide. During phase 2 the P3HT layer is (I) covered with PDMS still liquid properly degassed for 1 h), (II) heated at 80 °C for 12 h, (III) peeled off from the original substrate. In phase 3 the peeled layer is printed onto the new substrate and then the PDMS layer is detached from P3HT layer.

In the stretching experiments a stripe of PDMS inked by P3HT (5 × 15 mm) is fixed at the two 5 mm edges in a vice-like apparatus and then a measurable constant stretching is applied. The substrate to be printed is moved towards the stretched stamp from below and then pressed to put it into contact with the stretched P3HT layer to be printed. For the μCP with variable pressure, a measurable pressure is applied to the substrate + the inked stamp with a press. In all the experiments the sample is held at a temperature of 80 °C during the printing process. The printing duration was always of 5 min. For the stretched cases where unintentional pressure is applied, the pressure has been held constant and reproducible and can be quantified in one order of magnitude lower than the intentional pressure used for the variable pressure experiments. It should be noted that the P3HT layer is taken off from the original substrate, where it was deposited by spin coating, as solid layer; besides PDMS has been poured still liquid and previously degassed. For these reasons it is the PDMS that fits P3HT layer and not viceversa, maintaining the roughness of the original P3HT layer actually unaltered even in those cases where P3HT is pressed. All the annealing treatments of the printed P3HT layers have been performed in dry box at a temperature of 190–200 °C slightly below to the melting point of P3HT in order to maximize the P3HT chain mobility and re-organization.

2.2. XRD measurements

XRD data were obtained in air and at room temperature at the XRD1 beam-line of the ELETTRA Synchrotron in Trieste. The wavelength of the monochromatic beam was 0.1 or 1.2 nm. The beam size was 0.2 × 0.2 mm. The samples were oriented by means of a four-circle diffractometer with a motorized goniometric head and a MarResearch 165 mm CCD camera or a 345 mm Imaging Plate as detectors.

2.3. AFM measurements

Morphological characterization has been carried out with commercial AFM NT-MDT in semi-contact mode. Both height images and phase images have been simultaneously acquired. The typical parameters used are 50–60% of the original modulation amplitude as reference signal at the cantilever resonance. Thickness of the P3HT layers has been measured with AFM contact mode and fall between 30 and 35 nm.

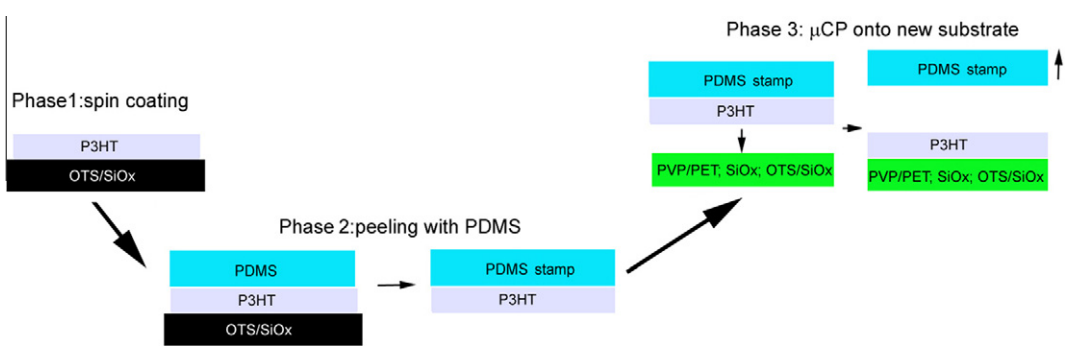

Fig. 1. Scheme of μCP deposition phases.

3. Results and discussion

3.1. Effect of stretching

The effect of μCP onto silicon oxide is shown in Fig. 2. The printed layer without stretching is essentially continuous and homogeneous (Fig. 2) and reproduces (inset Fig. 2) the original P3HT layer morphology of filaments randomly distributed typical of the P3HT deposited by spin coating onto silicon oxide [38–48]. The straight structures are compatible with a sequence of stacked P3HT molecules with the π orbital interacting with the neighbour macromolecules (see for example [41]). It is interesting to note that not only the morphology but also the roughness is generally preserved in the printing process compared to the spin coated P3HT film (roughness: 6–8 nm). This is due to the fact that PDMS fits to the P3HT layer and decorates it without influencing its organization.

The effect of the stretching of the deposited P3HT induced by the PDMS matrix is shown in Fig. 3. First of all, the homogeneity and compactness of the P3HT layer is a function of the applied elongation. By increasing the elongation ratio, defined as $\Delta = (l - l_0)/l_0$, the layer initially continuous and compact evolves, for a controlled cracking effect, into interconnected terraces delimited by empty areas predominantly oriented along the direction normal to the stretching direction. Fig. 3a shows the morphology corresponding to $\Delta = 0.1$ where the terraces are still adjoining and delimited by touching edges. By increasing elongation to $\Delta = 0.2$ (Fig. 3b), the formation of empty breaks in between interconnected terraces occurs even if the layer maintains its continuity. The voids are mostly oriented along the direction normal to the stretching direction. By further increasing Δ, Fig. 3c and d, the voids widen and the total amount of void areas increases. According to Fig. 4, the dependence void area/elongation is not linear: from $\Delta = 0.0$ to $\Delta = 0.4$, void amount increases by 0.3 times. From $\Delta = 0.4$ to $\Delta = 1.0$, the increase is only of 0.05 times. This means that, during PDMS_P3HT elongation, most of the changes in void density occurs in the transition from continuous to the onset of layer splitting while, for larger elongations, strain is already completely released and then the void density does not change appreciably. The average roughness and the island thickness (30–40 nm) remain approximately constant and independent of elongation ratio.

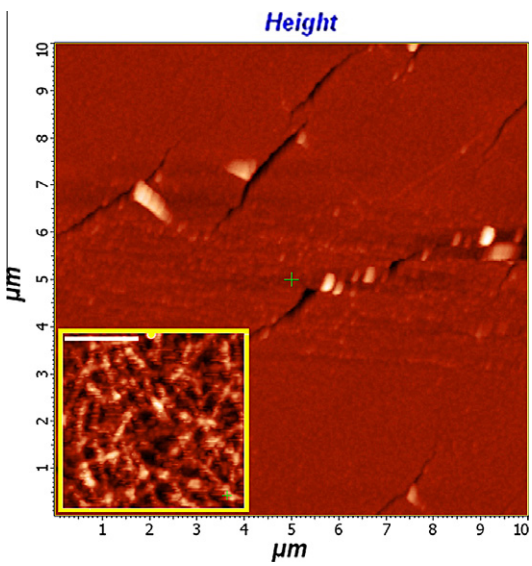

Fig. 2. Morphology of a P3HT layer printed on SiO_x without PDMS stretching. Inset: details of printed layer. White bar corresponds to 0.5 μm.

The effect of the annealing at a temperature close to the P3HT melting point (190 °C) is shown in Fig. 5 for the exemplary case of $\Delta = 0.2$. Annealing produces a more homogeneous re-organization of the voids, more dashed and distributed, and, at a more detailed level, the appearance of a homogeneous pore distribution (diameter 150–200 nm) that in the non-annealed case are hidden. This effects can be ascribed to P3HT chain mobility induced by the high temperature.

A second effect of the annealing following the stretching is to improve the overall crystallinity for moderate stretching ($\Delta = 0.2$) thus leading to a further formation of oriented fibrils, as a consequence of the previous strain, markedly as compared to non-annealed case.

Images of Fig. 6 reveal that the P3HT fibril orientation within the terraces along the stretching direction reaches the maximum at $\Delta = 0.2$. For Δ values > 0.4, the orientation sensibly decreases and at $\Delta = 1.0$ totally disappears thus coming back to non-stretched situation. In other terms, combination of elongation/post-annealing produces an efficient orienting effect towards the P3HT fibrils until the layer maintains its compactness. Whenever the strain implies a fragmentation of the P3HT layer into separate islands, the strain energy accumulation is released in the layer breaking and not in the fibril orienting process within the layer itself.

This last morphological result correlates with the XRD results according to which for low P3HT stretching (up to $\Delta = 0.4$), an *edge-on* orientation of high inter-fibril order/crystallinity is prevalent while for higher stretching a partial shift from *edge-on* to *face-on* orientation occurs thus indicating a higher disorder and a lower long range crystallinity (see below in the Section 3.1.1).

Finally, for $\Delta = 0.2$, annealing not only improves the crystallinity of single P3HT fibrils but induces the formation of rod-like crystallites (length of 1.2 micron and section of 100 nm in figure) oriented along the fibril direction, shown in Fig. 7. Unlike the height image (Fig. 7a), the phase images (Fig. 7b) reveal a multi-fibril composition of the structure coming from a pairing of different P3HT fibrils and/or a folding of the same fibril. These structures will occur again later (see Section 3.2) in the form of wires, as a consequence of a low mechanical pressure, although in that case they are more flexible.

A schematic representation of the morphological change induced by the stretching is shown in Fig. 8 where fibrils are represented by segments that before stretching are randomly oriented and after stretching are oriented along the stretching direction. A macroscopical quantity such as stretching is used to induce an ordering at nanometer level.

3.1.1. XRD results

Thin films printed from PDMS subjected to different elongation ratios, but not annealed, were examined by

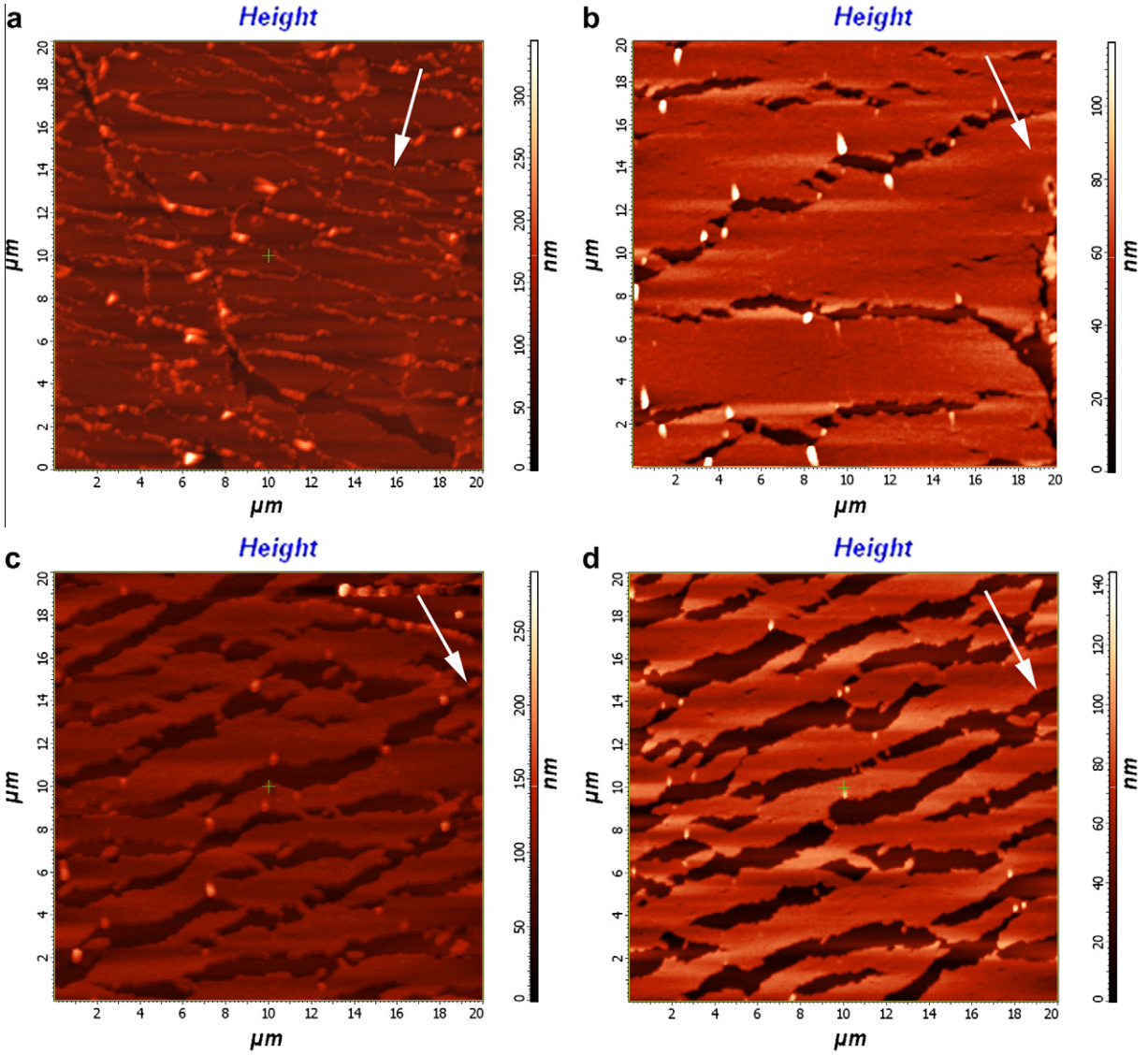

Fig. 3. morphological evolution of the P3HT layer printed from PDMS stamp function of the PDMS/P3HT elongation $\Delta = (l - l_0)/l_0$. (a) $\Delta = 0.1$, (b) $\Delta = 0.2$, (c) $\Delta = 0.4$, (d) $\Delta = 1.0$. Stretching direction indicated by white arrow in all the images.

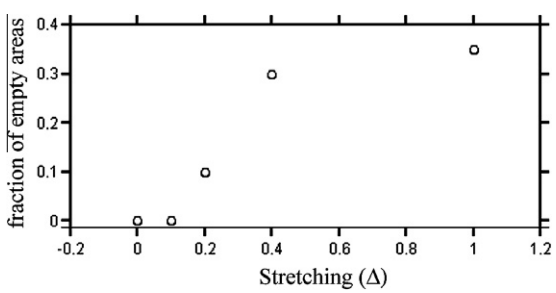

Fig. 4. Void/total area fraction as a function of the PDMS/P3HT elongation Δ. For each case measurements on five different areas have been analysed. Standard deviation falls within ±0.015 for all the values.

synchrotron radiation diffraction. The orientation model of P3HT together with 2D original images and related profiles in both out of plane (OOP) and in plane (IP) geometry are reported in Supplementary Part.

The first relevant observation from the analysis of data, which an exemplary 2D-image is reported in Fig. 9, is that OOP profiles exhibit [1 0 0] direction peaks mainly, conversely the IP data indicate the presence of (0 2 0) reflection only. These facts imply the essentially *edge-on* orientation of the macromolecules, as observed in thin films obtained by either spin coating or casting [38–48] Accurate analysis of the XRD data according to different incidence angles, using paracrystal approximation [51,52] gave no clear indication of any penetration depth trend, surely due to the insufficient crystallinity achieved. However, considering the parameters reported in Table 1, it is clear that the profiles along the direction parallel to the stretching are more neat than the perpendicular one, this

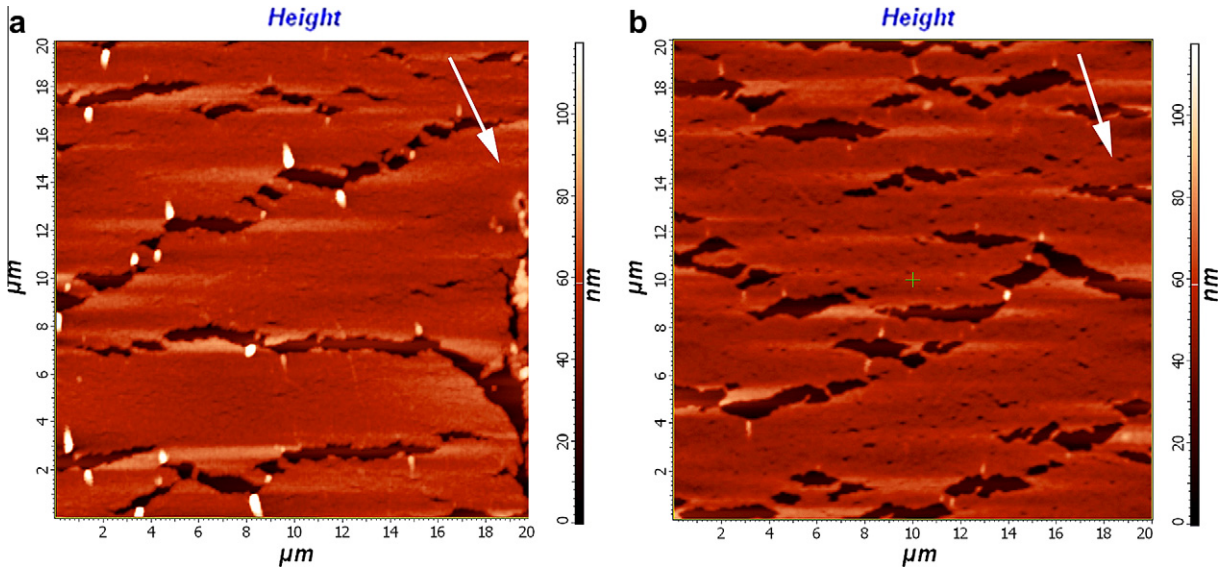

Fig. 5. Annealing effect on the layer morphology for elongation Δ = 0.2. Morphology (a) before and (b) after annealing. Stretching direction indicated by white arrow in both the images.

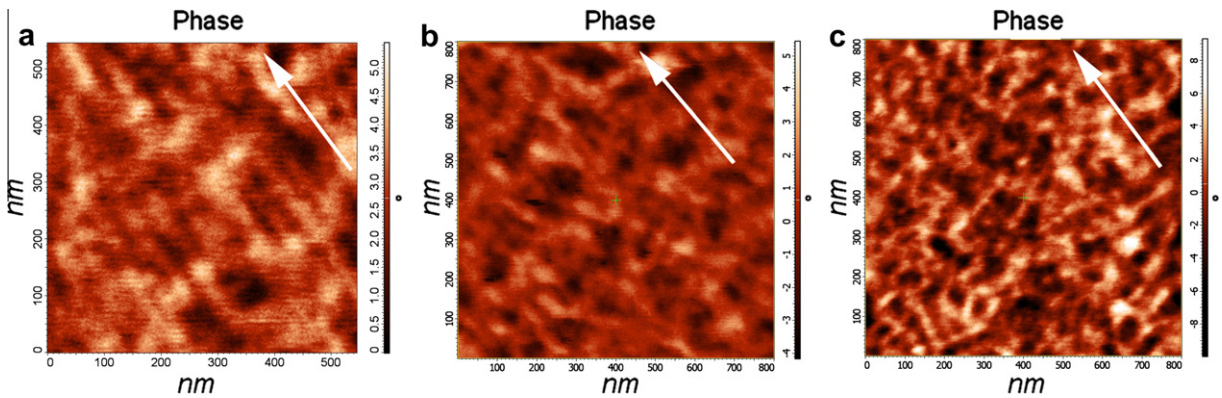

Fig. 6. Details of the annealed layers at different stretching Δ values: (a) Δ = 0.2, (b) Δ = 0.4, (c) Δ = 1.0. Stretching direction indicated by white arrow in all the images.

earning deep insights. Specifically the crystal size along [0 1 0] (IP scans) are larger in images taken parallel to the stretching direction (Fig. 9) than the ones recorded perpendicular to such a direction (not shown).

For a correct interpretation of these results, it is necessary to remind the model of the ultimate morphologic units (fibrils) of a deposited P3HT layer: each fibril consists of a sequence of macromolecules normal to the fibril elongation [38–48]. Considering the *edge-on* orientation of the chains, it is possible to definitely pinpoint the unit cell axes see for example [47,53] as exemplified in Fig. 10. Generally, these fibrils are randomly distributed onto the layer (see for example the inset of Fig. 2) but whenever a stretching is applied to the layer as shown before the effect of the stretching is an orientation of the fibrils along the stretching direction with respect to any other.

In these conditions, it is evident that when the XRD-beam is parallel to the stretching direction more macromolecules front-face orthogonally the impinging flux, respecting Bragg conditions for both (*h* 0 0) and (0 2 0) reflections; conversely in the case of the of flux normal to the stretching directions the macromolecules are crossed by XR-beam hence (0 2 0) reflection diffraction is hampered on the average. We like to remark that, due to low crystalline amount of the sample subjected to no thermal treatment, this result is necessarily qualitative, although pointing out a clear trend.

In synthesis, XRD results firstly confirm for the μCP P3HT layer a prevailing *edge-on* orientation with respect to the substrate, suggesting that such layers essentially are comparable to spin coated ones in terms of both orientation (*edge-on*) and morphologic features (fibril). Secondly, the higher crystallinity along the stretching direction as compared to the normal direction (i.e. higher OOP (1 0 0) peak intensity for vertical stacking and IP presence for horizontal π–π stacking) is consistent with the fibril orienting effect of stretching detected by AFM investigation.

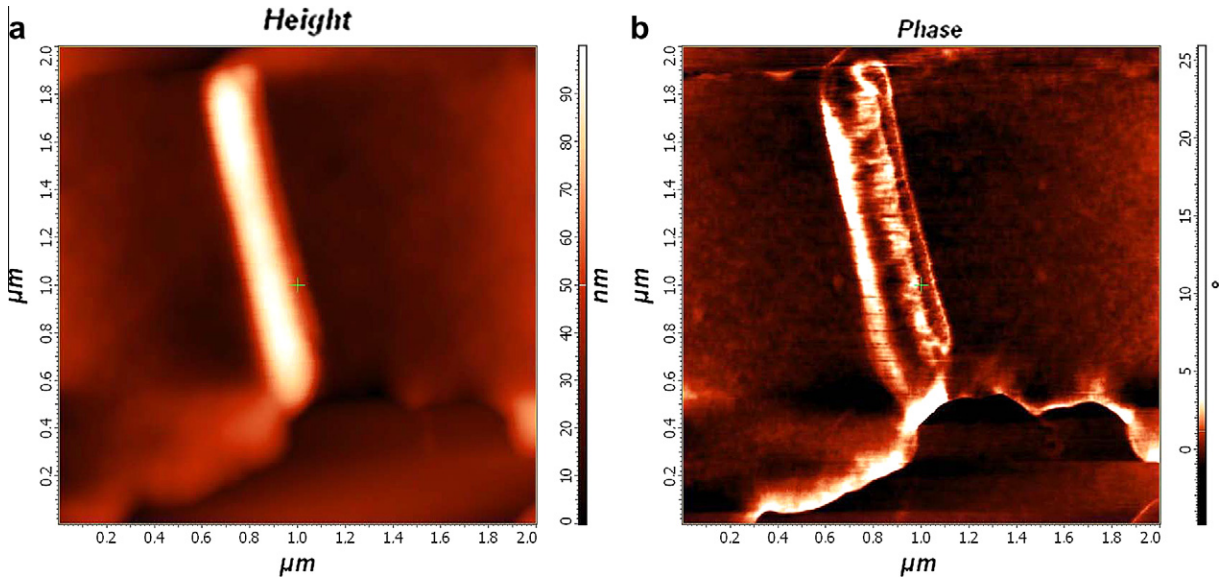

Fig. 7. Detail of rod-like structure for elongation Δ = 0.2. (a) Height and (b) phase image.

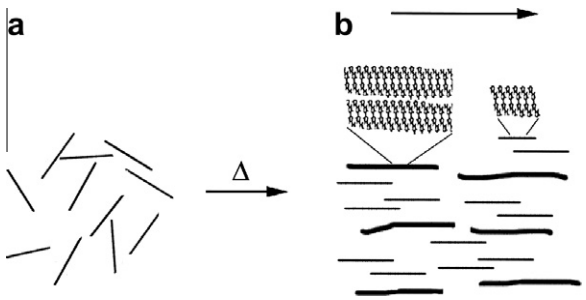

Fig. 8. Sketches representing the non-stretched (a) and stretched case (b). The thin black lines represent singular P3HT fibrils while the thicker black lines represent cohalescence of different P3HT fibrils induced by the orienting effect of the stretching.

Table 1
Structural parameters of selected thin films of P3HT stretched (40 nm).

Stretching direction	Peak profile			
	OOP		IP[a]	
	L (nm)[b]	$G_{100/200}$[c]	$G_{200/300}$[c]	L (nm)[b]
Parallel	8.6–9.4	3.0–3.6	3.0–3.2	4–6
Perpendicular	8.7–9.4	2.5–3.6	3.2	–[d]

[a] The intensity is small, especially for perpendicular direction.
[b] L is the average crystallite dimension as derived from Ref. [5]. The estimated standard deviation is close to 0.5 nm.
[c] G_{hkl} is the lattice fluctuation factor according to Hosemann paracrystal theory [4].
[d] Two broad peak, hence indeterminable.

Finally the effect of different stretching ratio (Δ) onto structural findings is fully in agreement with morphologic results above described. Namely, up to ratio values of Δ = 0.4 the crystallinity increases and also the orientation above this values no further increase are detected, rather the evidence of some *face-on* orientation – i.e. comparison of (0 2 0) along OOP profile and limitation of crystal size

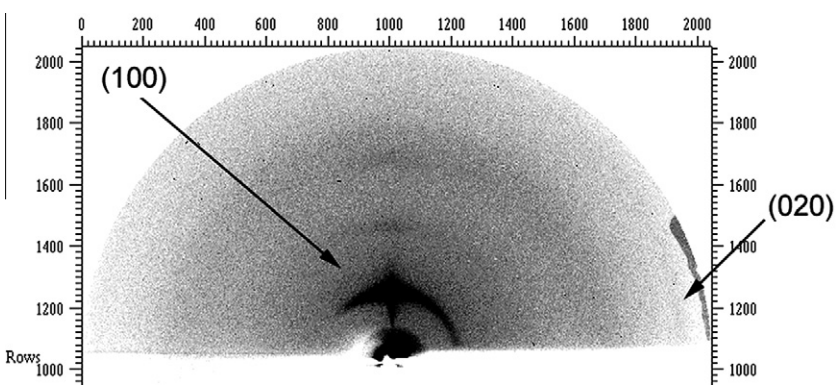

Fig. 9. XRD 2D-image of film (non-annealed) of P3HT printed onto silicon oxide, during stretching of PDMS (elongation Δ ~ 0.5). The beam flux is parallel to the stretching direction.

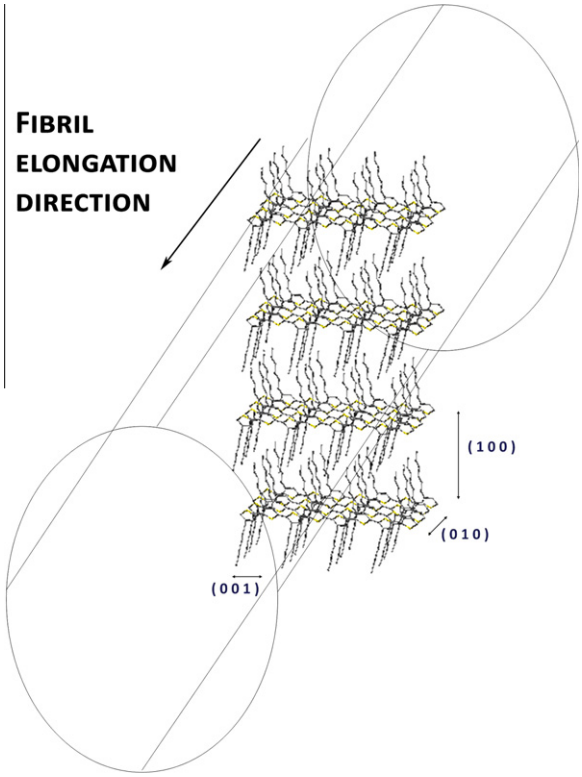

Fig. 10. Sketch of the crystalline part of the fibril with unit cell axis indicated, see text.

along [1 0 0] direction – is observed, probing significant misorientation, with respect to the substrate, during mechanical crystallization.

3.2. Effect of mechanical pressure onto the stamp

The effect of the mechanical pressure onto the stamp during the printing procedure is shown in Fig. 11 where AFM images reveal the morphology for the case without pressure, with a pressure of 0.3 and 0.6 N/cm^2.

The increase of pressure has a positive effect towards the layer compactness. Without pressure the layer is composed of adjoining, contiguous islands delimited by sequence of isolated small aggregates following the delimiting areas. The area occupied by the relief structures decorating the island edges represents approximately the 15% of the total area analysed. By applying an increasing pressure, the islands coalesce forming wider terraces and also the embossed delimiting lines tend to be absorbed and disappear. An approach more quantitative reveals that with an increase of pressure onto the stamp, the area occupied by relief structures decreases to 5% and to 1% for 0.3 and 0.6 N/cm^2 of pressure, respectively. Also the roughness decreases with an increasing pressure: going from no pressure to high pressure, the value halves (from 70 to 35 nm) thus confirming the observation that the layer terraces are more flat and the relieves thin out with the increasing pressure.

These remarks keep also validity for the cases where stretching is applied. Indeed, the previous stretched cases (for example Fig. 3) refer to a printing where a pressure is always applied simultaneously to stretching. On the contrary, Fig. 12 shows the case where μCP has been carried out without pressure. Relief structures that were absent in a previous case, now are present in terms of elongated macrofibrils/wires oriented along the stretching direction.

3.3. μCP onto a previously patterned silicon oxide

A similar situation occurs in Fig. 13 where a stretched μCP without pressure is used for deposition of a P3HT layer onto a previously patterned Au/SiO_x chip. In this specific case, the substrate consists of a sequence of Au arrays (6 μm wide separated by 2 μm) alternating to a bare silicon oxide surface. This patterning reproduces in a simplified way the morphology characteristic of a OFET device where the Au stripes are the electrodes while the layer in between represents the active organic layer specifically P3HT responsible for the OFET electron flux and mobility. Results, summarized in Fig. 13 for a stretched μCP ($\Delta = 0.2$) reveal the appearance of wire-like structures with variable section (from 80 to 150 nm (arrows Fig. 13b and c, respectively)) and variable length (100–2 μm) associable to a lateral coalescence of P3HT fibrils oriented along the stretching direction. Although wires are mostly straight and oriented, some of them are curved or circular (Fig. 13c double arrow). In some cases, the applied stretching is sufficient to create wires covering the whole distance between two electrodes (see white arrow in Fig. 13a). This fact, added to the orienting effect of P3HT fibrils seen in Fig. 7a, could have important implications in the electron mobility improvement.

3.4. Effect of substrate apolar character: OTS/Si oxide as a substrate

Up to now an oxidised Silicon single crystal has been used as final substrate where μCP occurs. Fig. 14 shows the effect of silicon oxide substrate silanization with OTS onto the final morphology. Under a stretching comparable to $\Delta = 0.2$, the layer undergoes to a breaking into different independent islands separated by channels, while in the silicon oxide case the fractures were more limited and only oriented in the direction normal to the stretching thus leaving a continuity and compactness of the layer.

This different behaviour can be attributed to a 'sliding' effect of the printed P3HT layer onto the apolar carpet due to OTS.

4. Conclusions

Micro-contact printing represents a solvent-free reproducible method to deposit a P3HT layer maintaining the typical fibril morphology and at the same time offering the opportunity to induce in the polymer layer crystallite ordering via fibril orientation and inter-fibril lateral pairing. This result can be obtained by applying a stretching to the PDMS stamp charged with the P3HT layer to be printed. A quantitative study in controlled conditions of the stretching effect towards the printed P3HT morphology

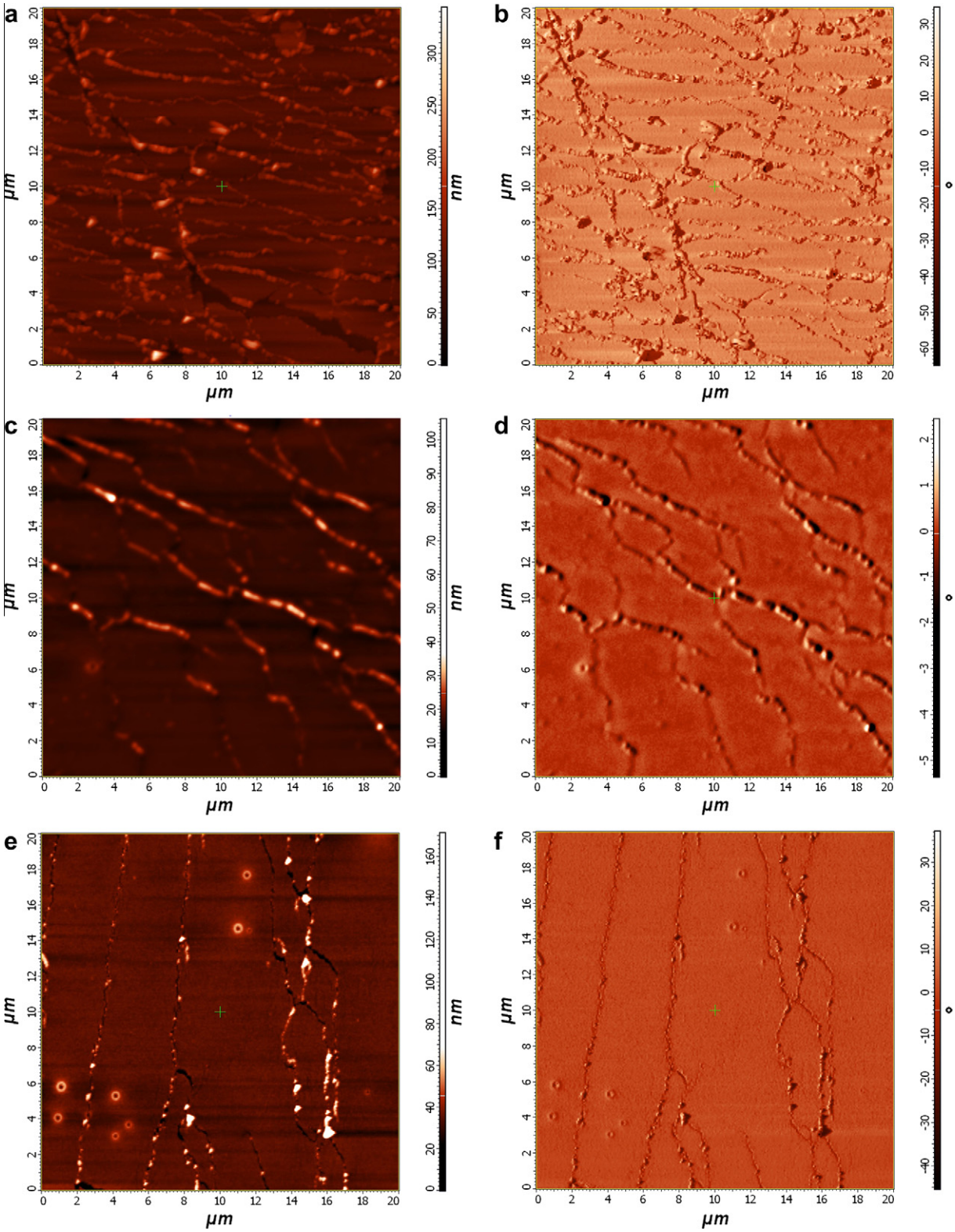

Fig. 11. Effect of mechanical pressure. Height and phase images for no pressure case (a and b, respectively), 0.3 N/cm^2 (c and d) and 0.6 N/cm^2 (e and f).

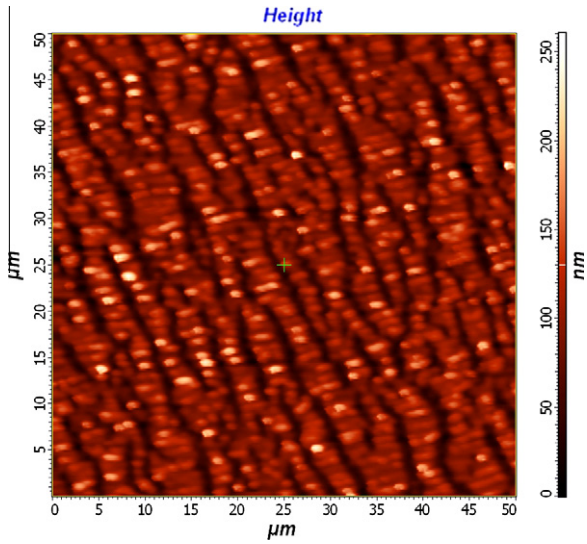

Fig. 12. Morphology of a stretched P3HT printed without pressure.

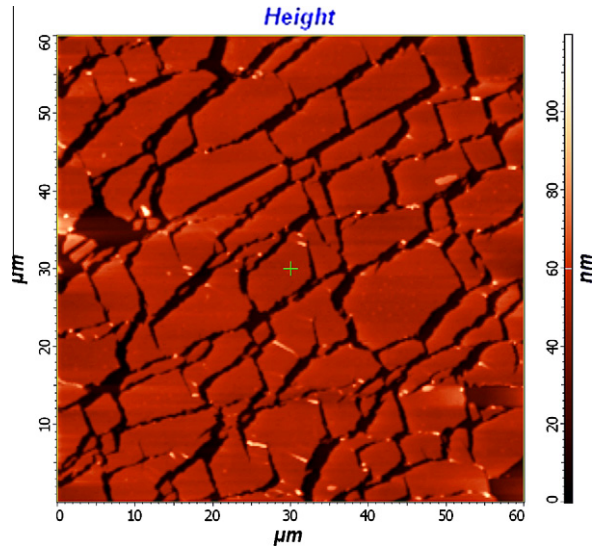

Fig. 14. Effect of the stretching for OTS as substrate.

indicates that stretching induces a controlled layer fragmentation and formation of channels in between interconnected islands. The percentage and shape of empty breaks is a function of the applied stretching hence it can be used to create nanochannels within a P3HT layer for templates. The combination of stretching and further annealing leads to an improvement of the overall crystallinity of the layer (XRD) and an orientation of P3HT fibrils along the stretching direction for elongation values able to still guarantee the layer compactness (max orientation at $\Delta = 0.2–0.3$). After such values significant mis-orientations (*face-on*) are evident through empty break formation. The μCP without mechanical pressure during the printing phase and with a simultaneous stretching allows the formation of wires probably due to a lateral pairing of different P3HT fibrils oriented along the stretching direction.

The stretching obtained with μCP has been shown to have an important role in orienting the P3HT fibrils responsible for the P3HT electron mobility of the active layer. In its turn, material orientation has been demonstrated by several authors to have an important role in improving the electron mobility [49,50].

The polar/apolar character of the substrate seems to assume an important role as driving force in addressing the morphology of the P3HT printed layer. In fact OTS–SAM onto treatment of Si oxide substrate modify the P3HT layer compactness, lowering the threshold to which it undergoes to definitive fragmentation along both the normal and parallel stretching direction thank to a sort of sliding effect onto OTS. However, silanization with OTS has been widely demonstrated to have a crucial role in improving the P3HT electron mobility due to its *edge-on* P3HT orienting effect [38–48]. In order to benefit of the 'horizontal' P3HT orienting effects of the stretching together with the OTS *edge-on* 'vertical' ordering of the starting spun film, it is mandatory to limit the stretching to values able to produce the positive orientation without counter-indication of layer breaking, i.e. $\Delta \leqslant 0.3$. Remarkably to remind is that the effect of

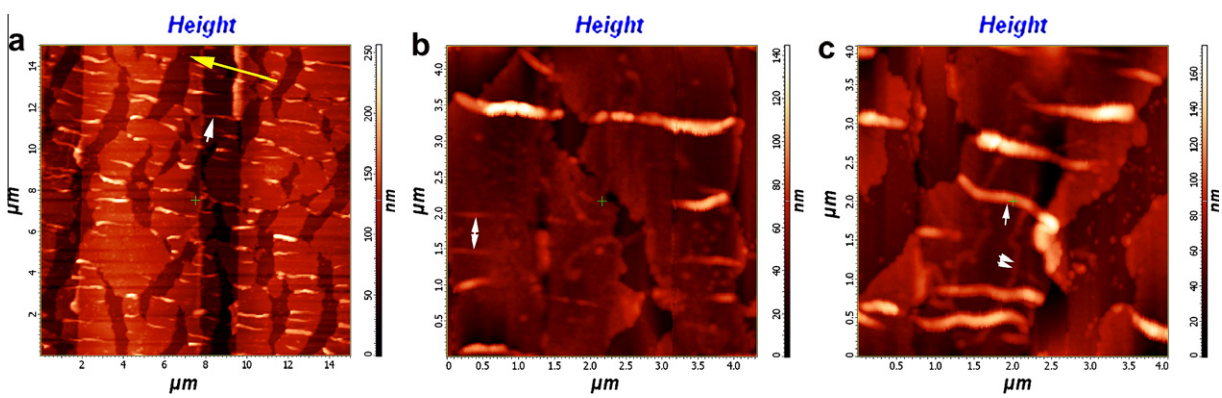

Fig. 13. Morphology of P3HT layer with stretching printed onto a patterned substrate. (a) General view. (b and c) Details. White arrows show examples of wire-like structures. Stretching direction indicated by yellow arrow in a). (For interpretation of the references to color in this figure legend, the reader is referred to the web version of this article.)

the polar/apolar character of the substrate needs to be investigated thoroughly in term of a wider spectra of silanizers exploring different degree of surface hydrophobicity to deep insight these qualitative results. Further investigations towards these directions are presently carrying on.

Acknowledgement

The authors thank MIUR and CNR for partial support through project PRIN 2007 "Materiali organici per dispositivi fotovoltaici ed elettroluminescenti: progettazione, sintesi, valutazione".

Appendix A. Supplementary data

Supplementary data associated with this article can be found, in the online version, at doi:10.1016/j.eurpolymj.2010.05.010.

References

[1] Gates BD, Xu Q, Stewart M, Ryan D, Grant Willson C, Whitesides GM. New approaches to nanofabrication: molding, printing, and other techniques. Chem Rev 2005;105(4):1171–96.
[2] Jacobs HO, Whitesides GM. Submicrometer patterning of charge in thin-film electrets. Science 2001;291:1763–6.
[3] Kumar A, Whitesides GM. Features of gold having micrometer to centimeter dimensions can be formed through a combination of stamping with an elastomeric stamp and an alkanethiol "ink" followed by chemical etching. Appl Phys Lett 1993;63(14):2002–5.
[4] Alom Ruiz S, Chen CS. Microcontact printing: a tool to pattern. Soft Matter 2007;3:168–77.
[5] Huck WTS. Self-assembly meets nanofabrication: recent developments in microcontact printing and dip-pen nanolithography. Angew Chem Int Ed 2007;46:2754–7.
[6] Xia Y, Whitesides GM. Soft lithography. Angew Chem Int Ed 1998;37:550–75.
[7] Menard E, Meitl MA, Sun Y, Jang-Ung Park, Jay-Lee Shir D, Yun-Suk Nam, et al. Micro- and nanopatterning techniques for organic electronic and optoelectronic systems. Chem Rev 2007;107:1117–60.
[8] Kagan CR, Breen TL, Kosbar LL. Patterning organic–inorganic thin-film transistors using microcontact printed templates. Appl Phys Lett 2001;79(21):3536–8.
[9] Helmuth JA, Schmid H, Stutz R, Stemmer A, Wolf H. High-speed microcontact printing. J Am Chem Soc 2006;128:9296–7.
[10] Yoo PJ, Choi S-J, Kim JH, Suh D, Baek SJ, Kim TW, et al. Unconventional patterning with a modulus-tunable mold: from imprinting to microcontact printing. Chem Mater 2004;16(24):5000–5.
[11] Luo C, Meng F, Liu X, Guo Y. Reinforcement of a PDMS master using an oxide-coated silicon plate. Microel J 2006;37:5–11.
[12] Packard CE, Murarka A, Lam EW, Schmidt MA, Bulovic' V. Contact-printed microelectromechanical systems. Adv Mater 2010;22:1–5.
[13] Bernard A, Renault JP, Michel B, Bosshard HR, Delamarche E. Microcontact printing of proteins. Adv Mater 2000;12(14):1067–70.
[14] Lee TW, Jeon S, Maria Zaumseil JJ, Hsu JWP, Rogers JA. Softcontact optical lithography using transparent elastomeric stamps: application to nanopatterned organic light-emitting divides. Adv Func Mater 2005;15:1435–9.
[15] Feng X, Meitl MA, Bowen AM, Huang Y, Nuzzo RG, Rogers JA. Competing fracture in kinetically controlled transfer printing. Langmuir 2007;23:12555–60.
[16] Paraskov R, Becker E, Riedl T, Johannes HH, Kowalsky W. Microcontact printing as a versatile tool for patterning organic field-effect transistors. Adv Mater 2005;17:1523–7.
[17] Marikkar FS, Carter C, Kieltyka K, Robertson JWF, Williamson C, Simmonds A, et al. Conducting polymer diffraction gratings on gold surfaces created by microcontact printing and electropolymerization at submicron length scales. Langmuir 2007;23:10395–402.
[18] Burdinski D, Saalmink M, van den Berg JPWG, van der Marel C. Universal ink for microcontact printing. Angew Chem Int Ed 2006;45:4355–8.
[19] Benor A, Hoppe A, Wagner V, Knipp D. Microcontact printing and selective surface dewetting for large area electronic applications. Thin Solid Films 2007;515:7679–82.
[20] Jeon NL, Finnie K, Branshaw K, Nuzzo RG. Structure and stability of patterned self-assembled films of octadecyltrichlorosilane formed by contact printing. Langmuir 1997;13(13):3382–91.
[21] Zschieschang U, Halik M, Klauk H. Microcontact-printed self-assembled monolayers as ultrathin gate dielectrics in organic thin-film transistors and complementary circuits. Langmuir 2008;24(5):1665–9.
[22] Liang Z, Li K, Wang Q. Direct patterning of poly(*p*-phenylene vinylene) thin films using microcontact printing. Langmuir 2003;19(14):5555–8.
[23] Jiang XP, Zhang H, Gourdin S, Hammond PT. Polymer-on-polymer stamping: universal approaches to chemically patterned surfaces. Langmuir 2002;18(7):2607–15.
[24] Qin D, Xia Y, Black AJ, Whitesides GM. Photolithography with transparent reflective photomasks. J Vac Sci Technol B 1998;16(1):98–103.
[25] Ng WK, Wu L, Moran PM. Microcontact printing of catalytic nanoparticles for selective electroless deposition of metals on nonplanar polymeric substrates. Appl Phys Lett 2002;81(16):3097–9.
[26] Zhiyong F, Ho JC, Jacobson ZA, Roie Yerushalmi, Alley RL, Razavi H, et al. Wafer-scale assembly of highly ordered semiconductor nanowire arrays by contact printing. Nano Lett 2008;8(1):20–5.
[27] Huck WTS, Yan L, Stroock A, Haag R, Whitesides GM. Duplication of photoinduced azo polymer surface-relief gratings through a soft lithographic approach. Langmuir 1999;15:6862–7.
[28] Jong-Hyun Ahn, Hoon-Sik Kim, Keon Jae Lee, Seokwoo Jeon, Seong Jun Kang, Yugang Sun, et al. Heterogeneous three-dimensional electronics by use of printed semiconductor nanomaterials. Science 2006;314:1754–7.
[29] Kraus T, Malaquin L, Schmid H, Riess W, Spencer ND, Wolf H. Nanoparticle printing with single-particle resolution. Nat Nanotechnol 2007;2:570–6.
[30] Cucinotta F, Popovic Z, Weiss EA, Whitesides GM, DeCola L. Microcontact transfer printing of zeolite monolayers. Adv Mater 2009;21:1142–5.
[31] Cao T, Xu Q, Winkleman A, Whitesides GM. Fabrication of thin, metallic films along the sidewalls of a topographically patterned stamp and their application in charge printing. Small 2005;1(12):1191–5.
[32] Loo YL, Willett RL, Baldwin KW, Rogers JA. Additive, nanoscale patterning of metal films with a stamp and a surface chemistry mediated transfer process: applications in plastic electronics. Appl Phys Lett 2002;81(3):562–4.
[33] Hur SH, Khang DY, Kocabas C, Rogers JA. Nanotransfer printing by use of noncovalent surface forces: applications to thin-film transistors that use single-walled carbon nanotube networks and semiconducting polymers. Appl Phys Lett 2004;85(23):5730–3.
[34] Chabinyc ML, Salleo A, Wu Y, Liu P, Ng BSO, Heeney M, et al. Lamination method for the study of interfaces in polymeric thin film transistors. J Am Chem Soc 2004;126:13928–9.
[35] Zhai L, Laird DW, McCullough RD. Soft-lithography patterning of functionalized regioregular polythiophenes. Langmuir 2003;19(16):6492–7.
[36] Park SK, Kim YH, Han JI, Moon DG, Kim WK. High-performance polymer TFTs printed on a plastic substrate. IEEE Trans Electron Devices 2002;49(11):2008–15.
[37] Liu B, Wang M, He Y, Wang X. Duplication of photoinduced azo polymer surface-relief gratings through a soft lithographic approach. Langmuir 2006;22:7405–10.
[38] Sirringhaus H, Tessler N, Friend RH. Integrated optoelectronic devices based on conjugated polymers. Science 1998;280:1741–4.
[39] Kline RJ, Mcgehee MD, Toney MF. Highly oriented crystals at the buried interface in polythiophene thin-film transistors. Nat Mater 2006;5:222–8.
[40] Kim DH, Jang Y, Park YD, Cho K. Layered molecular ordering of self-organized poly(3-hexylthiophene) thin films on hydrophobized surfaces. Macromolecules 2006;39:5843–7.
[41] Surin M, Leclère Ph, Lazzaroni R, Yuen JD, Wang G, Moses D, et al. Relationship between the microscopic morphology and the charge transport properties in poly(3-hexylthiophene) field-effect transistors. Appl Phys 2006;100(3):033712–6.
[42] Facchetti A, Yoon MH, Marks TJ. Gate dielectrics for organic field-effect transistors: new opportunities for organic electronics. Adv Mater 2005;17:1705–25.
[43] Forrest SR. The path to ubiquitous and low-cost organic electronic appliances on plastic. Nature 2004;428:911–8.

[44] Horowitz G. Organic field-effect transistors. Adv Mater 1998;10:365–77.
[45] Zhang R, Li B, Iovu MC, Jeffries ELM, Sauvé G, Cooper J, et al. Nanostructure dependence of field-effect mobility in regioregular poly(3-hexylthiophene) thin film field effect transistors. Am Chem Soc 2006;128:3480–1.
[46] Brinkmann M, Rannou P. Molecular weight dependence of chain packing and semicrystalline structure in oriented films of regioregular poly(3-hexylthiophene) revealed by high-resolution transmission electron microscopy. Adv Funct Mater 2007;17:101–8.
[47] Scavia G, Porzio W, Destri S, Barba L, Arrighetti G, Milita S, et al. Effect of the silanization and annealing on the morphology of thin Poly(3hexylthiophene) (P3HT) layer on silicon oxide. Surf Sci 2008;602:3106–15.
[48] Street RA, Northrup JE, Salleo A. Transport in polycrystalline polymer thin-film transistors. Phys Rev B 2005;71(16):165202 [1–13].
[49] Kim JS, Park Y, Lee DY, Lee JH, Park JH, Kim JK, et al. Poly(3-hexylthiophene) nanorods with aligned chain orientation for organic photovoltaics. Adv Funct Mater 2010;20:540–5.
[50] Coakley KM, Srinivasan BS, Ziebarth JM, Goh C, Liu Y, McGehee MD. Enhanced hole mobility in regioregular polythiophene infiltrated in straight nanopores. Adv Funct Mater 2005;15:1927–32.
[51] Hindeleh AM, Hosemann R. Microparacrystals: the intermediate stage between crystalline and amorphous. J Mater Sci 1991;26(19):5127–36. and ref. therein.
[52] Enzo S, Fagherazzi G, Benedetti A, Polizzi S. A profile-fitting procedure for analysis of broadened X-ray diffraction peaks. I. Methodology. J Appl Cryst 1988;21(5):536–40.
[53] Prosa TJ, Winokur MJ, Moulton J, Smith P, Heeger AJ. X-ray structural studies of poly(3-alkylthiophenes):an example of an inverse comb. Macromolecules 1992;25:4364–72.